

# Channeling of electrons and positrons in straight and periodically bent diamond(110) crystals

Alexander V. Pavlov<sup>1, 2</sup>, Andrei V. Korol<sup>3, 4</sup>, Vadim K. Ivanov<sup>1</sup>, and Andrey V. Solov'yov<sup>4 a</sup>

<sup>1</sup> Peter the Great St. Petersburg Polytechnic University, Polytechnicheskaya 29, 195251 St. Petersburg Russia

<sup>2</sup> Research Institute for Nuclear Problems, Belarusian State University, Bobruiskaya 11, 220030 Minsk Belarus

<sup>3</sup> St. Petersburg State Maritime University, Leninsky ave. 101, 198262 St. Petersburg Russia

<sup>4</sup> MBN Research Center, Altenhöferallee 3, 60438 Frankfurt am Main Germany

Received: date / Revised version: date

**Abstract.** In this paper we present the results of a systematic numerical analysis of the channeling properties for electrons and positrons in oriented straight and periodically bent diamond(110) crystals. We analyse the dependence of intensity of radiation emitted on the projectile energy as well as on the bending amplitude. The analysis presented is based on grounds of accurate numerical simulations of a channeling process. The simulation parameters, such as the crystal orientation, thickness and bending parameters of the crystals as well as the energy of the projectiles, were chosen to match those used in past and ongoing experiments. The peculiarities which appear in the radiation spectra are attributed to the interplay of various radiation mechanisms. The analysis performed can be used to predict and explain future experimental results.

**PACS.** 61.85.+p Channeling phenomena – 41.60.-m Radiation by moving charges – 41.75.Ht Relativistic electron and positron beams – 02.70.Uu Applications of Monte Carlo methods – 07.85.Fv X- and  $\gamma$ -ray sources, mirrors, gratings, and detectors

## 1 Introduction

Creation of new light sources is an important part of scientific progress. Nowadays, laser systems are capable of emitting electromagnetic radiation from infrared to X-ray range [1, 2]. However, creation of the devices able to emit photons with sub-angstrom wavelength is still challenging. Meanwhile, such light sources open a number of new possibilities for various scientific experiments and technological applications such as various medical applications, photon induced disposing of a nuclear waste and nuclear reaction [3–6].

One of the promising ways of generating sub-MeV - MeV photons relies on channeling of ultra-relativistic charged particles through oriented crystals. The basic effect of channeling in a straight crystal is in an anomalously large distance which a positively charged projectile penetrates moving along a crystallographic direction trapped in a potential well created by atomic planes or axes [7]. The particles which are trapped inside the potential well oscillate in the transverse direction while propagating in a planar or axial channel. The channeling oscillations result in a specific type of radiation - the channeling radiation

(ChR) [8]. Its intensity depends on the type of a crystal and the crystallographic direction, the type of a projectile and its energy [9–12].

Channeling also occurs in bent crystals, when the bending radius exceeds a critical value [13]. The motion in a bent crystal consists of two main components: the channeling oscillations and a circular motion along the bent channel center line. The latter gives rise to a synchrotron-type radiation [14]. The total spectrum of radiation emitted by an ultra-relativistic particle channeled in a bent crystal bears features of both the ChR and synchrotron radiation [15–17].

Another type of the radiation appears when an ultra-relativistic particle channels in a periodically bent crystal (PBC) [18, 19]. Such a system, called a crystalline undulator (CU), the undulator-type radiation (CUR) appears due to the periodicity in the projectile's trajectory which follows the shape of periodic bending. By changing the type of a projectile, the projectile energy  $\varepsilon$ , the crystal type and the bending parameters (such as the bending amplitude  $a$ , period  $\lambda_u$  and profile [20]) it is possible to tune the intensity and frequency of CUR. By using CU it is possible to achieve the peak brilliance of CUR up to  $10^{25}$  photons/s mrad<sup>2</sup> mm<sup>2</sup> 0.1%BW for photons in the energy range  $10^{-2} - 10^1$  MeV [20], such values cannot be achieved in the conventional undulators based on

<sup>a</sup> On leave from Ioffe Physical-Technical Institute, St. Petersburg, Russia.

Correspondence to: a.pavlov@physics.spbstu.ru

the magnetic field [21]. A systematic study of channeling and radiation parameters for various parameters of CU can open new opportunities for creation of new radiation sources.

In recent years, the study of the channeling phenomenon has attracted much of attention. A significant number of theoretical [17, 22–30] and experimental [31–40] works has been done to define the channeling parameters and electromagnetic radiation spectrum arising in the process. Additionally, several experiments have been performed aiming at detecting the CUR. The recent attempts include experiments with 195–855 MeV electron beam at the Mainz Microtron (MAMI) facility [31, 41] carried out with strained  $\text{Si}_{1-x}\text{Ge}_x$  superlattices [42, 43], experiments at SLAC with 10 – 35 GeV electrons and positrons of FACET beam [44, 45] and experiments with few-GeV positrons at CERN with PBC based on boron doped diamond [46]. Unfortunately, these attempts have not been entirely conclusive [47].

In order to make experimental studies more focused, additional theoretical analysis is required. In this work, we predict the evolution of the channeling properties and the radiation spectra for diamond(110) based CU [31]. Drastic changes in the radiation spectra with variation of the bending amplitude  $a$  of PBC are observed for different projectile energies  $\varepsilon$ . The changes are sensitive to the projectile's charge. The analysis presented predicts the results of experimental observations and allows us to design experiment in a way to get desired photon spectrum basing on the calculations.

## 2 Methodology and simulation parameters

In order to accurately predict experimental observations, one must rely on a software package which allows the accurate simulation of projectile motion in a crystalline environment. Because of that, MBN EXPLORER software package [48] was used to model the motion of ultra-relativistic projectiles through the crystalline medium along with the dynamic simulation of crystalline structures in a course of motion [49]. The computational framework of simulations is described in detail in Refs. [20, 49]. The computations account for the interaction of projectiles with separate atoms of the environment. The simulated trajectories were used to compute the spectra of electromagnetic radiation. This computational approach has been benchmarked previously in Refs. [20, 24, 49, 50].

In this work, the calculations were performed for electrons and positrons propagating in the oriented diamond (110) crystal. Interaction between the ultra-relativistic projectiles and the carbon atoms was simulated using the Molière potential [51]. The lattice temperature was set to 300K. The crystal and the particle's beam parameters were chosen to match the experimental conditions at the MAMI facility [31, 38]. Namely, the energy  $\varepsilon$  of the projectiles was considered within the range 270 – 855 MeV. The diamond crystal thickness  $L_{\text{cr}}$  was set to 20  $\mu\text{m}$ . The periodic bending was assumed to have a harmonic shape  $S(z) = a \cos(2\pi z/\lambda_u)$  where the coordinate  $z$  is measured

along the incident beam direction,  $\lambda_u$  is the bending period which was set to 5  $\mu\text{m}$ . Examples of the systems calculated in similar geometries can be found in Ref. [23]. All calculations were performed for the beams of particles with zero emittance. The particle trajectories and electromagnetic spectra were calculated for the straight crystal ( $a = 0$  Å) and for PBCs with following bending amplitudes  $a = 1.2, 2.5$  and  $4.0$  Å. For each simulation condition  $N = 6000$  trajectories were calculated. Statistical uncertainties due to finite numbers of the simulated trajectories correspond to the 99.9 % confidence interval (e.g. uncertainties which are shown by shaded area in the radiation spectra, Figs. 1, 2, 7(b), 8, were estimated as  $3.3 \sigma$  with  $\sigma$  being the standard deviation).

The radiation spectra of the particles were calculated according to the quasi-classical formalism by Baier and Katkov (see Ref. [52]). The comparison between the fully quantum approach and Baier and Katkov formalism [53] shows that the quasi-classical approach provides high calculation accuracy in application to the planar channeling problems. The emission spectra were carried out for the following two values of the detector opening angle:  $\theta_0 = 0.24$  mrad and  $\theta_0 = 4.0$  mrad. These values correspond to the apertures with diameter 4 and 40 mm at MAMI. The opening angles can be compared to the natural emission angles  $\gamma^{-1}$  ( $\gamma = \varepsilon/mc^2$  stands for the Lorentz factor): for  $\varepsilon = 270$  MeV  $\gamma^{-1} \approx 0.2$  mrad and for  $\varepsilon = 855$  MeV  $\gamma^{-1} \approx 0.6$  mrad. Thus, for both projectile energies the aperture with the opening angle  $\theta_0 = 4$  mrad collects almost all emitted radiation.

## 3 Obtained results

### 3.1 Radiation properties

One of the observables which can be measured in the channeling experiments with PBC is the spectrum of radiation emitted by the beam of particles [31]. A particle, channeled in a PBC, undergoes two types of quasi-periodic motion: the channeling oscillations and that due to periodicity of the bending. These motions bear close resemblance with the undulating motion. As a result, constructive interference of the waves emitted from the similar parts of the undulating trajectory are added together. For each value of the emission angle  $\theta$  the spectral distribution consists of a set of narrow and equally spaced peaks (harmonics). In the soft-photon limit, when the emitted energy  $\hbar\omega$  is small compared to the projectile energy  $\varepsilon$ , the frequencies of  $n$ th harmonic  $\omega_n$  of ChR or CUR can be found from the relation

$$\omega_n = \frac{2\gamma^2\Omega}{1 + \gamma^2\theta^2 + K^2/2}n, \quad n = 1, 2, 3, \dots, \quad (1)$$

where  $\Omega$  stands for the frequency of either channeling oscillations  $\Omega = \Omega_{ch}$  or the CU oscillations,  $\Omega = \Omega_u = 2\pi/\lambda_u$ .  $K^2$  is the mean square of the undulator parameter. In a CU, the motion of a particle consists of two independent quasi-periodic modes, therefore,  $K^2$  is given

by a sum of squared undulator parameters corresponding to different modes:  $K^2 = K_u^2 + K_{ch}^2$ , where  $K_u = 2\pi\gamma a/\lambda_u$  - the undulator parameter of a CU,  $K_{ch}^2 = 2\gamma^2\langle v_\perp^2 \rangle/c^2$  - the undulator parameter related to the channeling motion,  $\langle v_\perp^2 \rangle$  stands for the average velocity of the transverse motion (see Ref. [20] for details).

To estimate the dependence of ChR and CUR spectral densities on the bending amplitude  $a$ , one notices that spectral density,  $dE/\hbar d\omega \equiv I$ , of the radiation energy emitted by a bunch of particles experiencing a quasi-periodic motion is proportional to

- average number  $\langle N \rangle$  of particles participating in the motion,
- average distance  $L_{ch}$  covered by a particle,
- squared Fourier image of the particle's acceleration, which can be written as  $\Omega^4 A^2$  with  $\Omega$  and  $A$  standing for the frequency and the (average) amplitude of the quasi-periodic motion.

As a result one arrives at:

$$I \propto \langle N \rangle L_{ch} \Omega^4 A^2. \quad (2)$$

This estimate can be used to qualitatively explain the results of accurate calculations presented further in the paper.

The radiation spectra for the positrons and electrons with energies  $\varepsilon = 270$  and  $855$  MeV calculated for the opening angles  $\theta_0 = 0.24$  and  $4$  mrad are presented in Fig. 1 and Fig. 2, respectively.

Figs. 1(a),(e) serve reference purposes and illustrate well-established features of the emission spectra in straight crystals (see, e.g., Ref. [54]). For both electrons ('-') and positrons ('+') the spectra are dominated by the peaks of ChR, the spectral intensity of which by far exceeds that of the bremsstrahlung radiation in the amorphous medium (not shown in the figure). For positrons, nearly perfect harmonic channeling oscillations give rise to the narrow peak at  $\hbar\omega \approx 0.7$  MeV for  $\varepsilon = 270$  MeV and at  $\hbar\omega \approx 3.6$  MeV for  $\varepsilon = 855$  MeV. Due to the strong anharmonicity of the electron channeling oscillations, the peaks of ChR (marked with the upward arrows) are less pronounced and significantly broadened [54] (note the scaling factor  $\times 5$  applied to the electron spectra).

To comment on the spectra formed in PBC we first consider the smaller energy of projectiles,  $\varepsilon = 270$  MeV. In Figs. 1(b - d) the peak of CUR appears in both the electron and positron emission spectra at the energy  $\hbar\omega \approx 0.13$  MeV. The peak intensity increases with the bending amplitude in accordance with Eq. 2. On the contrary, the intensity of ChR exhibits moderate decrease as  $a$  increases. These patterns are similar for electrons and positrons.

For higher projectile energy,  $\varepsilon = 855$  MeV, the evolution of the spectra is less straightforward.

The most prominent feature in the positron spectra is a strong suppression of the ChR peak as  $a$  increases. Indeed, for  $a = 1.2$  Å, Fig. 1(f), the ChR peak intensity,  $I_{ChR}^{(+)}(a)$ , drops by a factor of two compared to the straight crystal. For larger bending amplitudes the ChR peak virtually disappears, Figs. 1(g - h).

In case of electrons, the modifications of the spectra are much peculiar. The peak of CUR have maximum as a function of  $a$  and become broader (more synchrotron like) for high bending amplitude (Fig. 1 (h)) The intensity of ChR  $I_{ChR}^{(-)}(a)$  for electrons does not fall off so dramatically as for positrons. The peak of ChR become more and more blueshifted with increase of  $a$  (note the position of upward arrows in Fig. 1) Additional peak appears in the high energy part of the radiation spectra of PBCs (Figs. 1 (f - h)).

These changes are associated with the dynamics of both channeled and dechanneled particles.

Channeled particles mainly contribute to the CUR and ChR radiation. The analysis of the behavior of channeled particles is presented in Section 4.2).

Dechanneled particles in a PBC are mainly involved in two processes: volume reflection (VR) [55,56] in the vicinity of points of maximum curvature and motion through parts of the crystal with small curvature and under small angles, i.e. the over-barrier motion as it defined in continuous potential approximation. These types of motion contribute to the different parts of radiation spectra. The first lies in the energy domain of the ChR for a given bending amplitude. The second is emitted at higher energies and reveals itself as additional peak on the radiation spectra. The possibility of radiation emission by over-barrier particles in the field of PBC was discussed qualitatively using the theory of continuous potential approximation in Ref. [57]. However, the analysis of such a phenomena using the accurate all-atom molecular dynamics provides more detailed information and predicts the effect not only qualitatively, but quantitatively. The analysis presented in the Section 4.3 reveals the contribution from the channeling and dechanneled particles to the radiation spectra.

The spectra obtained at  $\theta_0 = 4$  mrad bear close resemblance to one collected at the angle  $\theta_0 = 0.24$  mrad. For example, the spectra in Figs. 2(a) and 2(e) are dominated by the ChR. The evolution of CUR with  $a$  for electrons and positrons with  $a$  have same pattern. However, the left shoulders of the peaks are red-shifted because of the dependence of  $\omega_n$  on the collection angle (see Eq. 1). This broadening makes some of the features less distinguishable. For example, the additional high-energetic peak in the electron spectra is seen in the spectra for  $\theta_0 = 0.24$  mrad (Figs. 1 (b - d)), disappears for  $\theta_0 = 4$  mrad (Figs. 2 (b - d)). Additionally, larger opening angle leads to the larger spectral densities of radiation (note different scales in Figs. 1 and 2), the larger the opening angle, the more radiation enters the detector area [20]. Another interesting feature is that the radiation intensity for the positrons and electrons varies differently with changing of the aperture (scaling factor of the electron spectra  $\times 5$  for collection angle  $\theta_0 = 0.24$  mrad and factor  $\times 2$  for  $\theta_0 = 4$  mrad)

It is also worth noting, that in the positron emission spectra the higher harmonics occur in the spectra of CUR and ChR, the number and intensity of which changes with the energy of positrons. The spectral distributions of ChR and CUR with several harmonics for the positrons are clearly distinguishable from the smooth curves of the elec-

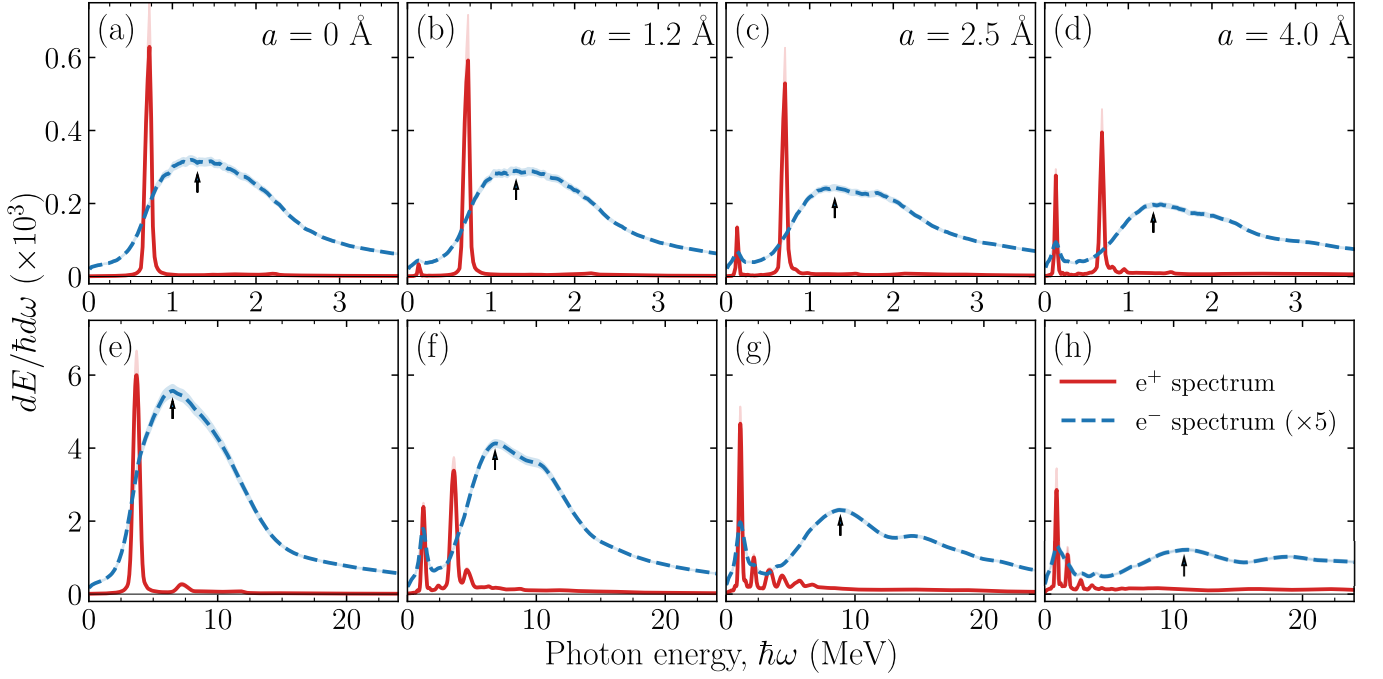


**Fig. 1.** Spectral distributions of radiation by 270 MeV (upper row, graphs (a) - (d)) and 855 MeV (lower row, graphs (e) - (h)) electrons (dashed blue curves) and positrons (solid red curves) calculated for the opening angle  $\theta_0 = 0.24$  mrad. First column, graphs (a) and (e), correspond to the straight crystal ( $a = 0$  Å). Other columns correspond to PBC with bending amplitudes 1.2, 2.5, 4.0 Å as indicated in the upper graphs. Note that the electron spectra are multiplied by factor of 5. Shading indicates the statistical error due to the finite number of simulated trajectories. The upward arrows show the positions the peaks due to ChR (in straight crystal) and due to interplay of ChR and additional emission due to volume reflection in PBC (see Section 4.3). For the sake of comparison we quote the intensities of the background incoherent bremsstrahlung estimated within the Bethe-Heitler approximation:  $2.9 \times 10^{-6}$  and  $2.5 \times 10^{-5}$  for  $\varepsilon = 270$  and 855 MeV, respectively.

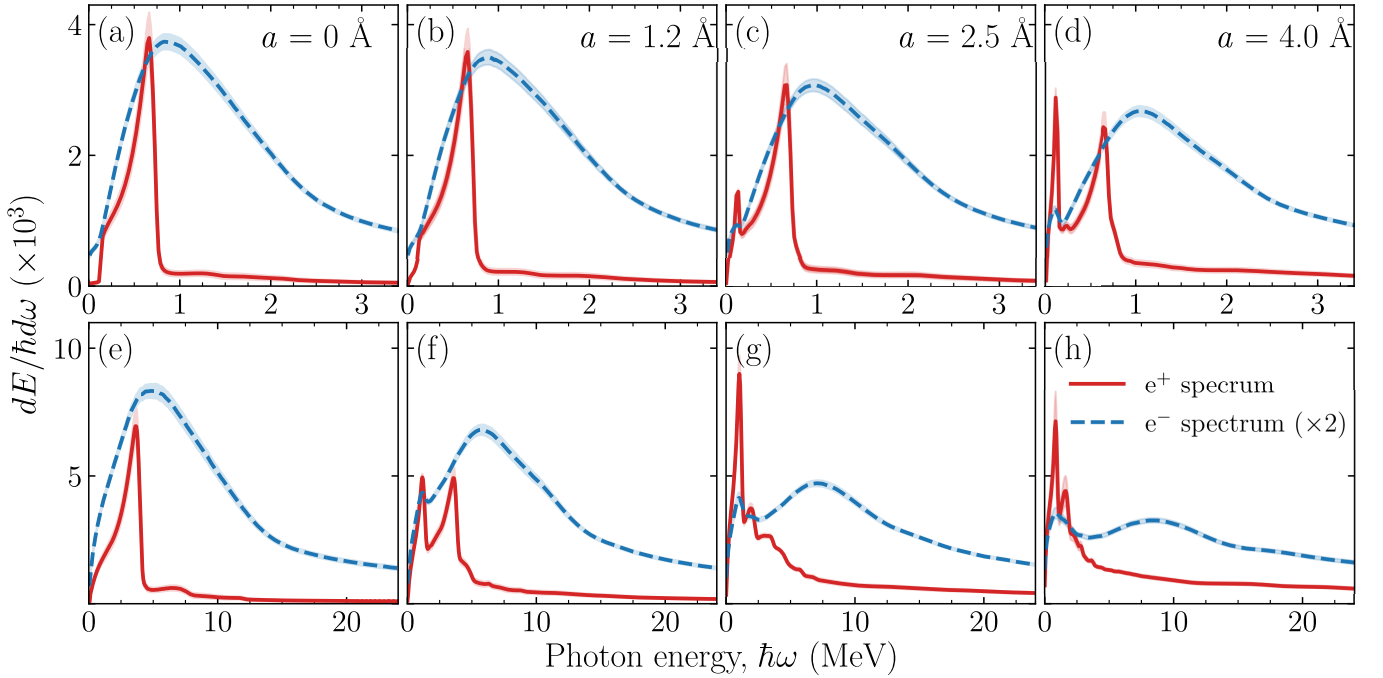


**Fig. 2.** Same as in Fig. 1 but for larger opening angle,  $\theta_0 = 4$  mrad. The electron spectra are multiplied by 2. The intensities of the background incoherent bremsstrahlung are  $1.3 \times 10^{-4}$  and  $1.8 \times 10^{-4}$  for  $\varepsilon = 270$  and 855 MeV, respectively.

tron spectra. For  $\varepsilon = 270$  MeV the additional harmonics of ChR are barely seen (note small bump in Fig. 1(a) around  $\hbar\omega \approx 2.1$  MeV), but for  $\varepsilon = 855$  MeV the higher harmonics are clearly seen both for the CUR (additional peaks in Fig. 1(e) around  $\hbar\omega \approx 7.5$  MeV) and the ChR (additional four equidistant peaks in Fig. 1(h)). This fact is in agreement with the theory of undulator radiation (see, e.g., [20,58]). It predicts that when the undulator parameter  $K \sim K_u = 2\pi\gamma \frac{a}{\lambda_u} \lesssim 1$ , emission spectra must contain few harmonics, the intensities of which rapidly decrease with the harmonic number  $n$ . Higher harmonics are more pronounced for lower apertures (see Fig. 1 (g) and Fig. 2 (g)).

### 3.2 Channelling properties

Ultrarelativistic electrons and positrons propagate in crystals in different potentials [20]. Positrons move in the smooth harmonic potential, in contrast, electrons move in the strongly anharmonic potential. Obviously, the different potentials result to the different channeling properties.

In the experiments, the particles can enter the crystal at any possible transverse coordinate. So, in our simulations initial values of the transverse coordinates of the particles must be randomized. Because of this and thermal fluctuation of the crystalline environment not all projectiles start moving inside a crystal in the channeling mode. A commonly used parameter to quantify the latter property is the acceptance defined as the ratio  $\mathcal{A} = N_{\text{acc}}/N$  of the  $N_{\text{acc}}$  number of particles that start motion in the channeling regime to the total number of particles  $N$ . The non-accepted particles experience unrestricted over-barrier motion at the entrance but can rechannel somewhere in the bulk. For different theoretical approaches to the interaction of the projectiles with the crystalline environments, the different criteria distinguishing channeling and non-channeling motions of the particles can be introduced. For example, in the continuous potential approximation the transverse (inter-planar) and the longitudinal motions of the projectiles are decoupled [7]. As a result, it is natural to define the channeling projectiles as those with the transverse energy not exceeding the height of inter-planar potential barrier. Within this framework, the acceptance  $\mathcal{A}$  is determined at the entrance of the crystal and is defined as the ratio of the number of the particles with the transverse energy less than the depth of potential well to the total number of the particles. In the simulations based on the solution of the equations of motion, a projectile interacts, as in the reality, with the individual atoms of the crystal [49]. The potential experienced by the projectiles varies rapidly in the course of their motion, that couples the transverse and the longitudinal degrees of freedom. Therefore, other criterion is required to select the channeling episodes of the projectile motion, i.e. the acts of acceptance and re-channeling. In that case one can assume channeling to occur when a projectile, while moving in the same channel, changes the sign of transverse velocity at least two times [49]. Thus, the acceptance  $\mathcal{A}$

is determined not at the entrance but at some distance inside the crystal.

Using above approach it is possible to introduce the characteristic lengths of channeling motion. The average distance which an accepted particle passes inside a crystal before the dechanneling is called the penetration length  $L_p$ . The mean distance which particle pass inside a crystal in channeling mode is often called de-channeling length  $L_{\text{ch}}$ . In relatively thick crystal multiple events of the channeling - dechanneling - re-channeling can occur. So, to determine the total distance which particles propagate inside a crystal in the channeling regime one can introduce a total channeling length  $L_{\text{tot}}$ . The total channeling length  $L_{\text{tot}}$  can be calculated by averaging the length of all channeling segments over the total number of trajectories  $N$ .

The parameters which characterize electron and positron channeling in the crystals with different bending amplitudes  $a$  are presented in Table 1.

The acceptance  $\mathcal{A}$  and the total channeling length  $L_{\text{tot}}$  are maximal in straight crystal and then gradually decrease with bending amplitude  $a$ . This can be explained using a simple but illustrative model of continuous potential: effective potential drops with increase of bending amplitude due to the centrifugal force [54]. The acceptances are relatively same in the straight crystal for  $\varepsilon = 270$  and 855 MeV, but drop with  $a$  significantly faster for  $\varepsilon = 855$  MeV, because of the higher growth rate of the centrifugal force. The acceptance is larger for positrons than for electrons. This fact can be explained in a following way: in an oriented crystal a projectile electron, being attracted to an atomic plane, gains the transverse energy via the harder collisions with the crystal constituents and, thus, switches to the over-barrier motion much faster than a positron which experiences (on average) softer collisions. Because of almost harmonic potential, positrons have much larger channeling length  $L_{\text{ch}}$  compared to electrons and once a positron is accepted, it channels without dechanneling, but despite electrons the re-channeling events (capturing of the particle to the channel after free movement inside the crystal [20]) for positrons are rare. The channeling length, however, growth linearly with a projectile energy (see Eq. 6.3 and 6.4 in Ref. [20]), which leads to higher channeling lengths in straight crystal for projectiles with energy 855 MeV. The evolution of the channeling lengths with  $a$  is very similar to the evolution of acceptance where increase in the centrifugal force leads to the strong suppression of the depth of potential well. For example for 270 MeV electrons  $L_{\text{tot}}(a = 0 \text{ \AA})/L_{\text{tot}}(a = 4.0 \text{ \AA}) \approx 2$  and  $\approx 1.3$  for positrons, in contrast, for 855 MeV electrons the ratio  $\approx 4.7$  and  $\approx 3.2$  for positrons.

For more information about the channeling properties, parameters and visualization of the channeling trajectories see for example Ref. [17] section 3.1 and Ref. [20] chapter 6. Comparison between the experimental and theoretical data one can find, for example, in Ref. [31].

**Table 1.** The acceptance  $\mathcal{A}$ , penetration length  $L_p$  and total channeling length  $L_{tot}$  for electrons and positrons with energy  $\varepsilon = 270$  and  $855$  MeV in the straight and periodically bent diamond(110) crystal. The first column indicates the bending amplitude  $a$  ( $a = 0$  corresponds to the straight crystal). The second column shows the maximal bending parameter  $C$  for corresponding projectile energy and bending amplitude. Condition  $C = 4\pi^2 a \varepsilon / \lambda_u^2 U'_{\max} < 1$  allows one to estimate whether or not channeling can effectively occur ( $U'_{\max} = 6.7$  GeV/cm the maximum gradient of interatomic potential for diamond at room temperature [20]). The last column represents the peak intensity of CUR  $I_{CUR}^{(+)} (\times 10^3)$  for positrons with certain energy.

$a$ (Å)	$C$	$\mathcal{A}$	$L_p$ (μm)	$L_{tot}$ (μm)	$\mathcal{A}$	$L_p$ (μm)	$L_{tot}$ (μm)	$I_{CUR}^{(+)} (\times 10^3)$
$\varepsilon = 270$ MeV								
Electrons $e^-$					Positrons $e^+$			
0	0	0.70	$5.32 \pm 0.21$	$8.85 \pm 0.29$	0.96	$18.84 \pm 0.18$	$18.42 \pm 0.27$	0.002
1.2	0.07	0.61	$4.90 \pm 0.20$	$7.62 \pm 0.25$	0.93	$18.53 \pm 0.21$	$17.78 \pm 0.32$	0.034
2.5	0.15	0.51	$4.26 \pm 0.19$	$5.96 \pm 0.19$	0.88	$18.76 \pm 0.19$	$17.06 \pm 0.32$	0.134
4.0	0.24	0.40	$3.72 \pm 0.17$	$4.29 \pm 0.13$	0.76	$18.16 \pm 0.24$	$14.65 \pm 0.38$	0.277
$\varepsilon = 855$ MeV								
Electrons $e^-$					Positrons $e^+$			
0	0	0.72	$10.85 \pm 0.32$	$11.72 \pm 0.32$	0.96	$19.24 \pm 0.14$	$18.87 \pm 0.21$	0.03
1.2	0.23	0.48	$7.25 \pm 0.33$	$7.89 \pm 0.28$	0.83	$18.94 \pm 0.17$	$16.71 \pm 0.40$	2.38
2.5	0.48	0.30	$4.98 \pm 0.28$	$4.46 \pm 0.14$	0.60	$16.77 \pm 0.30$	$11.96 \pm 0.48$	4.67
4.0	0.77	0.21	$3.51 \pm 0.17$	$2.42 \pm 0.06$	0.26	$14.55 \pm 0.61$	$5.92 \pm 0.34$	2.83

## 4 Discussion

### 4.1 Positron channeling

Let us now analyze the case of positron channeling. In the planar channeling regime, a charged projectile moves along a planar direction experiencing a collective action of the electrostatic field of lattice atoms [7]. For a positively charged projectile, the atomic field is repulsive, so that the particle is steered into the inter-atomic region and oscillates (channels) in between two adjacent crystalline planes. At some stage, due to the collisions with the crystal constituents, the transverse energy becomes large enough to allow particle to leave the channeling mode, i.e. to dechannel. The opposite process, the re-channeling, is associated with the capturing to the channeling mode. In a sufficiently thick crystal, a projectile can experience dechanneling and re-channeling several times in the course of propagation. In this case, the quantity  $\langle L \rangle$  in Eq. 2 should account for the length of all channeling segments in the trajectory  $L_{tot}$ . However, for the crystals shorter than the dechanneling length the re-channeling events are rare [17, 20, 23, 24]. The positrons with energy of several hundreds MeV have channeling length  $L_{ch} \gg 100 \mu\text{m}$  [59], so in that case  $\langle L \rangle$  can be calculated as the mean penetration  $L_p$  length (this value is depicted in column 7 of Table 1). Correspondingly, the value  $\langle N \rangle$  can be associated with the number of accepted particles, which is related to the acceptance  $\mathcal{A}$  (column 6 of Table 1).

These data allows one to qualitatively analyze the dependence of the intensity of the CUR  $I_{CUR}^{(+)}$  on  $a$  in case of positrons. Using Eq. 2 and taking into account that the factor  $\Omega_u^2$  is independent on the amplitude, one writes:  $I_{CUR}^{(+)}(a) \propto \mathcal{A}(a)L_p(a)a^2$ . Here, the term  $\mathcal{A}(a)L_p(a)$  is a decreasing function of the bending amplitude, in combination with  $a^2$ , resulting function  $I_{CUR}^{(+)}(a)$  have the max-

imum at some value of the bending amplitude (see the last column of Table 1). The maximum at  $a = 2.5$  Å is clearly seen for  $\varepsilon = 855$  MeV, but for  $\varepsilon = 270$  MeV the dependence  $I_{CUR}^{(+)}(a)$  constantly growth for all observed  $a$ , so the maximum should appear at large bending amplitudes than those studied in this work.

Similar methodology is applicable to the analysis of dependence of ChR intensity  $I_{ChR}^{(+)}$  on  $a$ . In this case, assuming the harmonic character of channeling oscillations, i.e. the independence of frequency  $\Omega_{ch}$  on the amplitude of challenging oscillations  $a_{ch}$ , one writes Eq. 2 as follows:  $I_{ChR}^{(+)} \propto \mathcal{A}(a)L_p(a)\langle a_{ch}^2 \rangle(a)$ . Here,  $\langle a_{ch}^2 \rangle(a)$  stands for the mean square amplitude of channeling oscillations. This quantity is a decreasing function of bending amplitude. Indeed, as  $a$  increases the centrifugal force, especially in the vicinity of the points of maximum curvature, drives the projectiles, oscillating with large amplitudes, away from the channel. This results in the strong quenching of channeling oscillations.

Fig. 3 shows the probability densities for a particle to have a certain channeling amplitude, which is important for the analysis of the emission spectra of these particles. These dependencies do not show the average deviation of the particle from the center of the channel. Instead, they are defined as  $(\Delta N(a)/\Delta a)/N_{tot}$ . Here  $\Delta N(a)$  is the number of oscillations with the amplitude within the interval  $\Delta a$ ,  $N_{tot}$  – is the total number of oscillations (i.e. with any  $a$ ). It should be noted that the amplitude of oscillations is defined as the maximum deviation of the channeling particle from the center of equilibrium. Additionally, the fact that the center of potential shifts due to the centrifugal force (see Eq. A.25 in [20]) was taken into account. Thus, the distributions were obtained as follows. For each channeling particle, the distance from the equilibrium line were measured at the moment when the particle changes

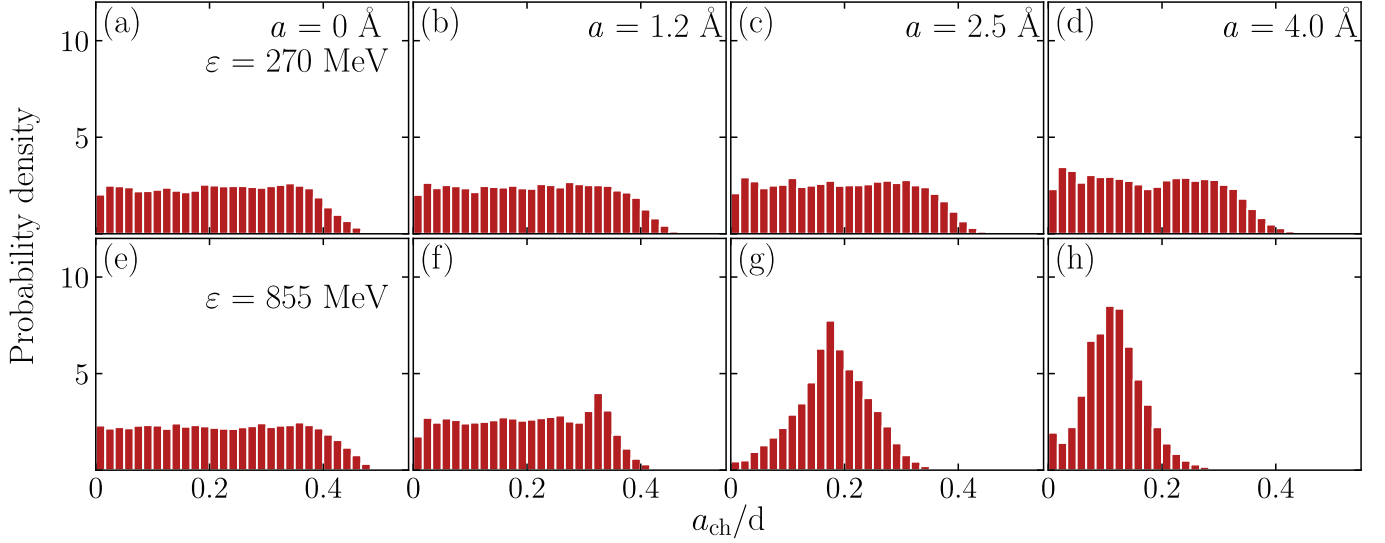


**Fig. 3.** Probability density distributions over channeling amplitudes  $a_{\text{ch}}$  for positrons with energies 270 and 855 MeV. (a) - corresponds to case of the straight crystal case (bending amplitude  $a = 0$ ) and energy  $\varepsilon = 270$  MeV, (b)-(d) - corresponds to channeling in PBC with bending amplitudes  $a = 1.2, 2.5$  and  $4.0$  Å correspondingly, (e)-(h) same as (a)-(d) but for positrons with energy  $\varepsilon = 855$  MeV

the sign of its velocity. After this, this procedure was repeated for all channeling sections of all particles. Based on the obtained values, the presented distributions are constructed. In this way, the presented distributions are obtained for channeling events throughout the depth of the crystal.

In case of a straight crystal, the particles are distributed uniformly over all possible oscillation amplitudes. The nature of this phenomenon stems from the quasi-harmonicity of the interatomic potential for positrons. However, with increase of the bending amplitude, changes in the distribution occur. For the positrons with energy  $\varepsilon = 270$  MeV (Figs. 3(a – d)) the increase of  $a$  leads to the small decrease in the maximum possible amplitude and small reorganization of entire distribution.

For the positrons with energy  $\varepsilon = 855$  MeV (Figs. 3(e – h)) the values of centrifugal forces are larger than for  $\varepsilon = 270$  MeV, so distributions possess much more complicated evolution. The probability density distribution for the PBC with  $a = 1.2$  Å looks similar to the distributions for  $\varepsilon = 270$  MeV. Slight decrease in the channeling amplitude results in the small reorganization of the distribution. In case of  $a = 2.5$  and  $4.0$  Å (Figs. 3(g, h)) distributions have pronounced peak. This behavior can be explained in a way that the centrifugal force moves potential minima closer to the point of maximum curvature, another words, the center of potential starts to shift inside the channel. In this situation positrons cannot precisely follow the minima of potential, so constant shift in the positron trajectories appears. The peak in Figs. 3(g, h) moves to lower values with increase of  $a$ , because particles with higher channeling amplitudes have higher probability to be kick-out from the channel.

Summarizing above results let us conclude that the gradual decrease in all three factors,  $\mathcal{A}$ ,  $L_p$  and  $\langle a_{\text{ch}}^2 \rangle$  re-

sults in the considerable drop in the intensity of ChR: the value of  $I_{\text{ChR}}^{(+)}$  at  $a = 4$  Å is by a factor of 30 less than for the straight channel, which is in accordance with the trend seen in Fig. 1 and 2.

Another approach that can explain the behavior of ChR spectra is based on the analysis of fast Fourier (FFT) spectra of the particles trajectories. This approach allows one to visualize the impact of bending amplitude on the amplitude of channeling oscillations  $\Omega_{\text{ch}}$ . On such dependence amplitude of oscillations  $a_{\text{ch}} \propto \text{FFT intensity}$  and frequencies  $\Omega_{\text{ch}} \propto \text{Fourier frequency}$ .

Examples of FFT spectra are presented in Fig. 4. The presented spectra are averaged over all particle that are moved through the crystal without dechanneling. Fig. 4 organized as follows: the FFT spectra are for positrons with energy  $\varepsilon = 270$  MeV are shown on the left, spectra for  $\varepsilon = 855$  MeV positrons are shown on the right. Fig. 4 (a) shows the FFT spectra for the straight crystal, in this case spectra consist of peaks (the red shading) which corresponds to the channeling oscillations. For the positrons with energy  $\varepsilon = 270$  MeV oscillation frequencies lie between  $f = 0.8 - 1.2 \mu\text{m}^{-1}$ , however for positrons with energy  $\varepsilon = 855$  MeV oscillations have frequencies between  $f = 0.4 - 0.8 \mu\text{m}^{-1}$ . Difference in the frequency can be calculated using simple model (see e.g. chapter 4.2 in Ref. [20]) where  $\Omega_{\text{ch}} \sim \sqrt{U'/dm\gamma}$ ,  $U'$  is the first derivative of the interplanar potential. Using above analysis one can get ratio  $\Omega_{\text{ch}}(270)/\Omega_{\text{ch}}(855) = \sqrt{\gamma(855)/\gamma(270)} \approx 1.8$ . This value fits the observed results.

In Figs. 4(b – d), corresponding to the PBCs, the FFT signals at  $f = 0.2 \mu\text{m}^{-1}$  correspond to the motion along the cosine centerline with the period  $\lambda_u = 5 \mu\text{m}$ . These peaks are normalized via division by  $a$ . By comparing the spectra within the interval indicated in the red shading for the straight and PBCs one sees the modification of the dis-



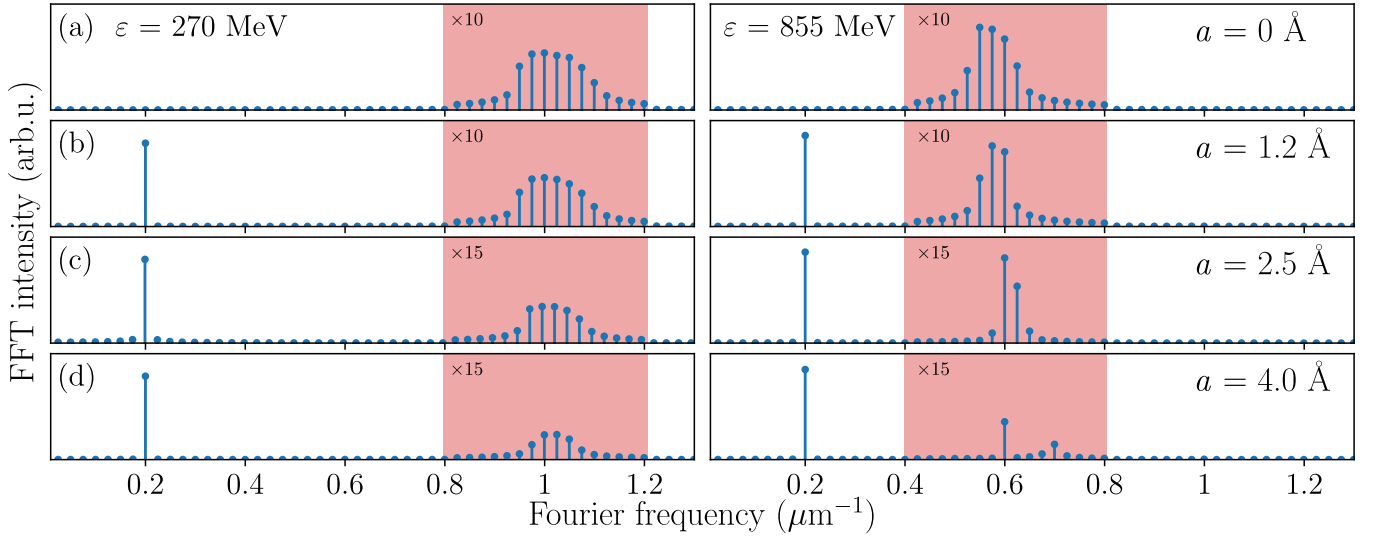


**Fig. 4.** The FFT spectra of trajectories for positrons with energies 270 (left) and 855 MeV (right) which is channeled through the whole  $L = 20 \mu\text{m}$  thick diamond(110). Graphs (a)-(d) refer to the straight crystal ( $a = 0$ ) and PBC with different  $a = 1.2, 2.5$  and  $4.0 \text{ \AA}$ , correspondingly. The red area shows the part of the spectrum due to the channeling oscillation (note the scaling factor 10 for (a), (b) and 15 for (c), (d)).

tribution of channeling oscillations. For two energies spectra modify in two ways: for lower energy with increase of  $a$  the intensity of channeling oscillations drops almost uniformly for all frequencies, for higher energy intensity of channeling oscillations quenches. In particular, the FFT spectra clearly indicate that with increase in the bending amplitude the ChR intensity decreases significantly, literally, only the oscillations on one frequency survives. So, the FFT spectra clearly indicate that with the increase in bending amplitude the ChR intensity decreases significantly for  $\varepsilon = 855 \text{ MeV}$  and uniformly drops for  $\varepsilon = 270 \text{ MeV}$ .

To conclude the discussion of positron case, let us remark once again the dependence of radiation spectra on the projectile energy. Figs. 1 and 2 show the emission spectra for two different  $\varepsilon$  and set of  $a$ . With increase in  $a$ , the ChR peak for the  $\varepsilon = 855 \text{ MeV}$  projectiles virtually disappears, whereas for lower  $\varepsilon = 270 \text{ MeV}$  it is still well pronounced. This effect is visible for both small  $\theta_0 = 0.24 \text{ mrad}$  and large  $\theta_0 = 4 \text{ mrad}$  opening angles and depends only on the strength of centrifugal force.

## 4.2 Electron channeling

Let us turn back to the emission spectra of electrons in Figs. 1 and 2. The dechanneling length  $L_{\text{ch}}$  of electrons in the straight diamond(110) is less than the crystal thickness  $L = 20 \mu\text{m}$ . In case of PBC,  $L_{\text{ch}}$  is even less being a decreasing function of  $a$ . To illustrate the differences in  $L_{\text{ch}}$  for positrons and electrons as well as the dependencies on  $a$ , one can, firstly, compare the values of  $L_p$  for electrons (column 4) and positrons (column 7) in the Table 1. Main contribution to the low-energy part of the spectrum, where CUR dominates, is made by the accepted particles.

To analyze the evolution of the CUR peak in the electron spectra, let us start from Eq. 2 and then follow the arguments outlined in the positron case. Finally one can get following relation:  $I_{\text{CUR}}^{(-)}(a) \propto \mathcal{A}(a)L_p(a)a^2$ . Similar to the positron case, the equation above is applicable when  $L_p(a)$  contains at least one CU period.

Analyzing the data from Table 1 one can notice that for the electrons with energy  $\varepsilon = 855 \text{ MeV}$  above statement is true only for  $a = 1.2$  and  $2.5 \text{ \AA}$ , this explains the difference in the CUR intensities in such crystals (Figs. 1(f, g) and Figs. 2(f, g)). However, for PBC with  $a = 4.0 \text{ \AA}$  the electrons with energy  $\varepsilon = 855 \text{ MeV}$  have penetration depth less than one period  $L_p < \lambda_u$ . This leads to the fact that for PBC with  $a = 4 \text{ \AA}$ , the radiation becomes more synchrotron-like. This manifests itself in the broadening of CU peak accompanied by additional reduction in peak intensity (see Fig. 1 (h) and Fig. 2 (h)).

For the lower energy electrons  $L_p \approx \lambda_u$  for all bending amplitudes. To better illustrate this fact, let us look at the dependencies of the primary fraction of electrons on penetration distance. The dependencies for  $\varepsilon = 270 \text{ MeV}$  are shown in Fig. 5 (a), as one can notice for all bending amplitudes the primary fraction virtually disappears between 5 and  $10 \mu\text{m}$ . This means that for all bending amplitudes only a small fraction of electrons participate in the collective motion inside CU. This fact leads to the conclusion, that the spectral density of CUR should increase with bending amplitude, since  $a^2$  growth faster, than  $\mathcal{A}(a)L_p(a)$  decreases. For  $\varepsilon = 855 \text{ MeV}$  (Fig. 5 (c)) the behavior is different, the number of primary electrons on certain distance strongly depends on the bending amplitude.

Let us now analyze the part of spectrum where ChR dominates. In this part of the spectrum the contribution



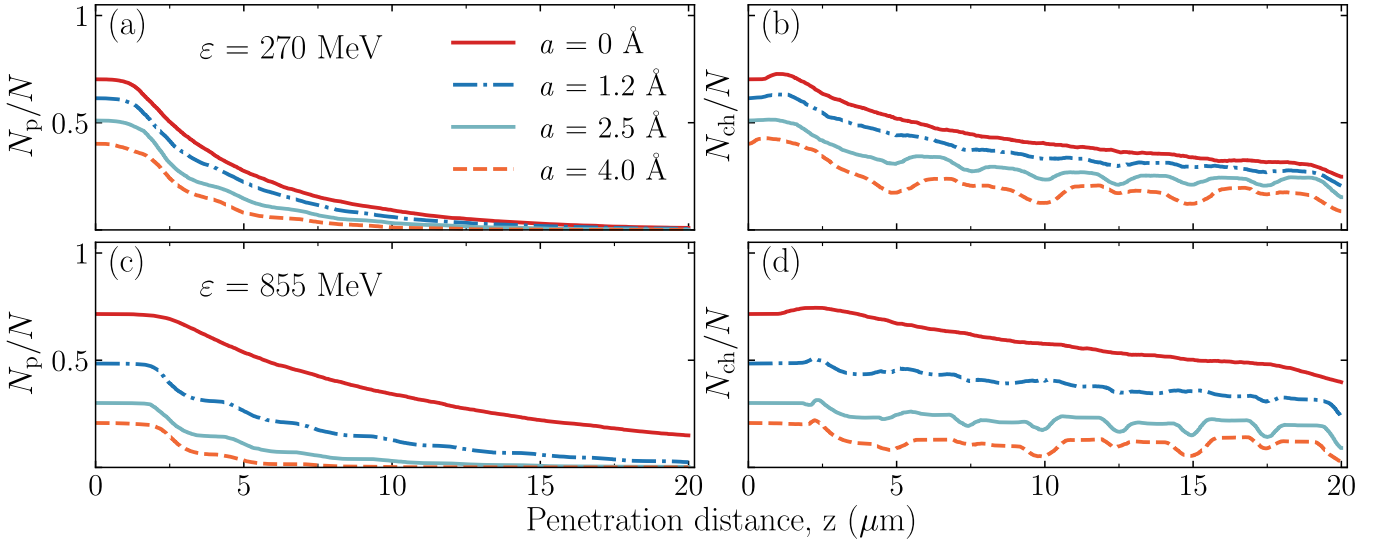


**Fig. 5.** Fraction of channeling electrons in straight ( $a = 0$  Å) and PBC diamond(110) crystal. (a) primary fractions of the accepted particles for energy  $\varepsilon = 270$  MeV, (b) fractions with account for the re-channeling for electrons with energy  $\varepsilon = 270$  MeV, (c) - (d) same as (a) - (b) but for electrons with energy  $\varepsilon = 855$  MeV

of the re-channeled particles to the electron emission spectrum increases.

The interplay of several processes, occurring in the PBCs, leads to the structural transformations in this part of the spectrum. This radiation is emitted by all particles experiencing the channeling motion. These include the accepted electrons as well as those re-channeled anywhere inside the crystal. It was shown in Ref. [23] that periodicity in the bending significantly enhances the re-channeling rate even in the limit of large bending curvatures  $1/R_{\max}$ . At the distances with maximum curvature (the minima and maxima of the cosine bending profile), the dechanneling rate is the largest, this results to the minima of channeling fraction  $N_{\text{ch}}/N$ . In contrast, at the distances where the curvature approaches zero value, the re-channeling yields a significant increase in the number of channeling electrons. The dependence of  $N_{\text{ch}}/N$  on  $z$  allows one to calculate the total length  $L_{\text{tot}}$  of all channeling segments per a projectile. The corresponding data are presented in the fifth column of Table 1.

For the cosine bending profile, particles enter the PBC in the point of maximum curvature. The centrifugal force filters the electrons with respect to their channeling amplitudes  $a_{\text{ch}}$ , so similar to the positron case the *accepted* particles oscillate with comparatively small amplitudes.

To illustrate this, the probability distributions of  $a_{\text{ch}}$  are shown in Fig. 6. The distributions for electrons were obtained in the same way as distributions for positrons. The distributions have asymmetric peak structure, where the lowest amplitudes are suppressed due to the scattering on a nuclear and the highest amplitudes are suppressed by the enhancement of de-channeling probability on the top of potential well. The predominance of small amplitudes can be explained by the fact that the anharmonicity of channeling oscillation (see, e.g., Refs. [24, 54]) leads to the fact that low-amplitude oscillations occur with a higher

frequency. As a result, the number  $\Delta N(a)$  of small amplitude oscillations is larger than the number of oscillations with large amplitudes. Those, on average, they happen more often than the large amplitude oscillations. This is valid for both straight and bent crystals. In Figs. 6(a – d) the distributions for  $\varepsilon = 270$  MeV are shown, since for all observed bending parameters  $C \ll 1$ , distributions change slightly with the increase in the bending amplitude. For  $\varepsilon = 855$  MeV (Figs. 6(e – h)) changes are much more pronounced and increase in bending amplitude of PBC results in the significant reduction of  $a_{\text{ch}}$ . The emission frequency is related to  $\Omega_{\text{ch}}$  as  $\omega_{\text{ch}} \approx 2\gamma^2\Omega_{\text{ch}}$ , one can conclude that the ChR spectrum of the accepted particles in PBCs is blue-shifted in comparison with the straight one, and this shift growth with the bending amplitude. The shift must be more pronounced for  $\varepsilon = 855$  MeV than for  $\varepsilon = 270$  MeV. This feature is seen in Figs. 1(a – h) where the upward arrows mark the positions of the ChR maximum. The account of the emission from the re-channeled electrons allows one to explain why the ChR spectrum does not decrease with  $a$  so dramatically as it happens in the case of positrons. Indeed, the re-channeling events occur on the (nearly) straight parts of the PB channel, where the centrifugal force is small. Therefore, the channeling amplitude  $a_{\text{ch}}$  of these particles is uniformly distributed within the interval  $a_{\text{ch}} \lesssim d/2$  giving rise to the emission into the whole interval of the ChR energies. As a result, the low-energy part of the ChR is non-zero for all amplitudes considered, and the ratio of the maximum values of the intensity with good accuracy follows the ratio of the  $L_{\text{tot}}$  values.

To conclude, the dechanneling–re-channeling dynamics together with the strong anharmonicity of the channeling oscillations lead to the modifications in the shapes of the electron emission spectra. These changes are significantly different from those discussed for the positrons.

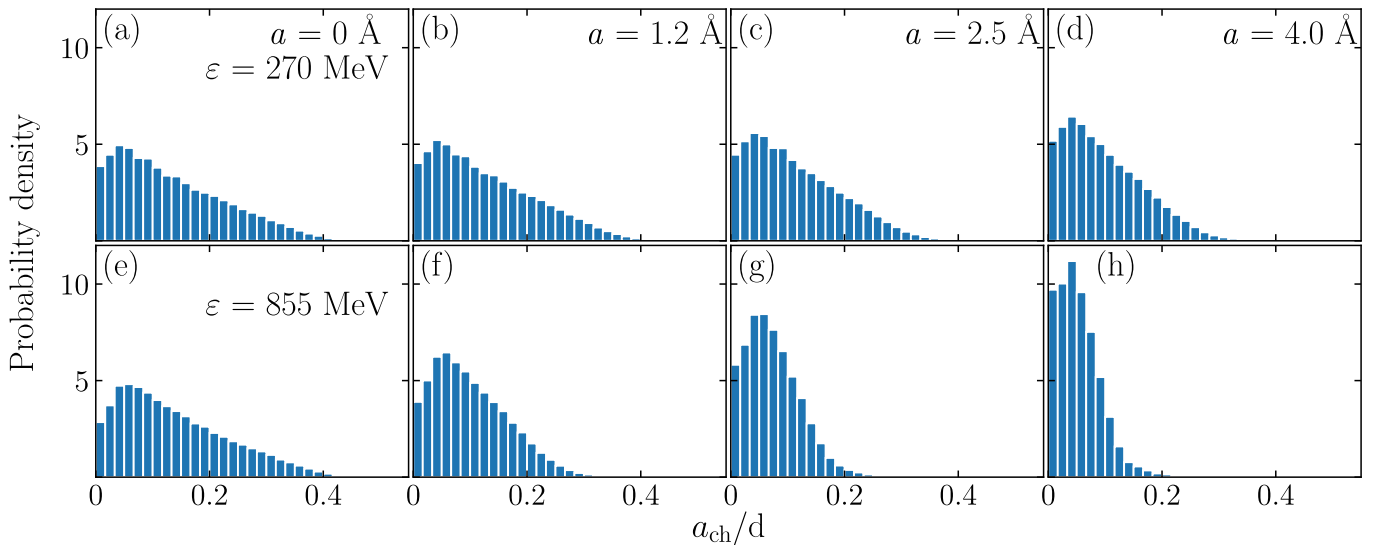


**Fig. 6.** Probability density distribution over channeling amplitudes  $a_{ch}$  for electrons with energies 270 and 855 MeV. (a) - corresponds to straight crystal case (bending amplitude  $a = 0$ ) and energy  $\varepsilon = 270$  MeV, (b)-(d) - corresponds to channeling in PBC with bending amplitudes  $a = 1.2, 2.5$  and  $4.0$  Å correspondingly, (e)-(h) same as (a)-(d) but for electrons with energy  $\varepsilon = 855$  MeV

### 4.3 Radiation by dechanneled electrons

Let us now analyze the contribution to the emission spectra of electrons due to dechanneled particles. Explicitly, this contribution reveals itself as an additional peak in the emission spectra from a PBC. This feature is more pronounced for 855 MeV electrons and appears in the spectra for  $a = 1.2$  Å as a bump just beyond the powerful maximum of ChR, see Fig. 1(b). It becomes more pronounced and shifted to higher energies as  $a$  increases, Fig. 1(c, d). In what follows we present the analysis of the role of different types of the motion experienced by channeling and non-channeling particles in formation of the emission spectrum.

To compare the contributions to the total emission spectrum coming from channeling and non-channeling particles the following procedure has been adopted. Each simulated trajectory has been divided into segments corresponding to different types of motion. Namely, we distinguished the following parts of the trajectory: (i) the channeling motion segments, (ii) segments corresponding to the over-barrier motion across the periodically bent crystallographic planes, (iii) segments corresponding to the motion in the vicinity of points of maximum curvature where a projectile experiences volume reflection [55, 56]. For each type of the motion, the spectrum of emitted radiation has been computed as a sum of emission spectra from different segments. Thus, the interference of radiation emitted from different segments has been lost.

The aforementioned procedure is illustrated by Fig. 7. Its upper panel, (a), presents two selected trajectories of 855 MeV electrons propagating in PBC with bending amplitude  $2.5$  Å. Different types of segments are highlighted in different colour and type of the line as indicated in the caption. The emission spectra corresponding to different types of motion (calculated accounting for

all simulated trajectories) are shown in the lower panel (b). The dependences presented allow one to associate the maxima in the total spectrum (black solid curve) with the corresponding type of motion. The radiation emitted from the segments of channeling motion (dashed green curve) govern the spectrum in the vicinity of the CUR peak ( $\hbar\omega_{CUR} \approx 1$  MeV) and provides a great contribution to the ChR,  $\hbar\omega_{ch} \approx 6 \dots 12$  MeV. Numerical analysis of the simulated trajectories has shown that the curvature of the trajectories segments in the points of VR is close to that of the channeling trajectories. As a result, the radiation from the VR segments is emitted in the same energy interval as ChR so that the peak centered at  $\approx 9$  MeV is due both to the channeling motion and to the VR events. The over-barrier particles experience quasi-periodic modulation of the trajectory when crossing the periodically bent channels. The (average) period of these modulation is smaller than that of the channeling motion and decreases with the increase of the bending amplitude. For  $a = 2.5$  Å this period is approximately two times less than the (average) period of channeling oscillations. As a result, radiation emitted from the over-barrier segments (dashed-dotted blue curve) is most intensive in the range  $\hbar\omega_{ch} \approx 15 \dots 20$  MeV. This contribution results in the additional structure in the total spectrum.

To illustrate the evolution of the contributions from the channelling and non-channeling particles to the emission spectrum with bending amplitude, we present Fig. 8. Graph (a) corresponds to the straight crystal, graphs (b)-(e) - to PBC with  $a = 1.2, 2.5, 4.0$  and  $5.5$  Å, respectively. Each graph presents the total spectrum, solid curve, the contribution of the channeling segments, dashed curve, and the contribution from the non-channeling segments (both over-barrier and VR), dash-dotted curve.

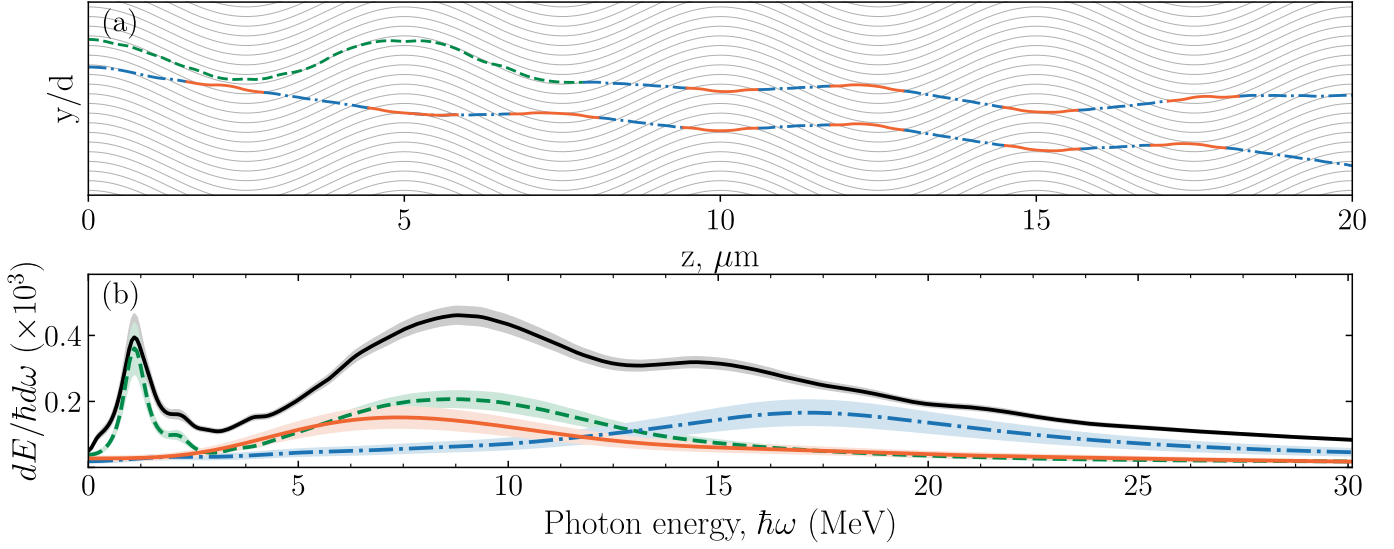


**Fig. 7.** (a) Selected simulated trajectories of 855 MeV electrons in a PBC bent with  $a = 2.5$  Å. Highlighted are the segments corresponding to the challenging regime (green dashed lines), over-barrier motion (blue dashed-dotted line) and to VR events (solid orange line). Thin wavy lines mark the atomic planes. (b) Spectral distributions of radiation emitted by a beam of 855 MeV electrons in the PBC. Solid black curve indicates the total spectrum. Dashed green, dashed-dotted blue and solid orange curves show the contribution from the segments of the channeling motion, over-barrier motion and due to the VR, respectively. The data refer to the opening angle  $\theta_0 = 0.24$  mrad.

First, we discuss the modification of the spectra in the photon energy range far beyond the CUR peak.

In the straight crystal as well as in the PBC with small bending amplitude ( $a = 1.2$  Å) the emission spectrum is dominated by the channeling particles which provide main contributions to the ChR peak. As  $a$  increases, the role of the non-channeling segments becomes more and more pronounced whereas the channeling particles contribute less. The increase in  $a$  leads to (i) increase of the curvature of a particle's trajectory in the vicinity of the VR points, (ii) decrease in the period of the quasi-periodic modulation of the trajectories of over-barrier particles. As a result, two maxima seen in the graphs (b)-(e) become blue shifted as  $a$  increases: the maxima marked with upward arrows are due to the channeling motion and to the VR, those marked with downward arrows are associated with the over-barrier particles. For large bending amplitudes, graphs (d)-(e), these maxima are virtually due to the emission of the non-channeling particles only.

The low-energy part of the spectrum formed in PBC is dominated by the peak located at  $\hbar\omega \approx 1$  MeV. For moderate amplitudes,  $a \leq 2.5$  Å, when the bending parameter  $C \ll 1$  (see Table 1), this peak associated with CUR and is due to the motion of the accepted particles which cover a distance of at least one period  $\lambda_u$  in a periodically bent channel. For larger amplitude,  $a = 4.0$  Å ( $C = 0.77$ ), the penetration length  $L_p$  of the accepted particles become less than half a period leading to noticeable broadening of the CUR peak. For even larger amplitudes, one notices further modifications of the peak which are related to the phenomenon different from the channeling in a periodically bent crystal. Graph (e) shows the dependences for  $a = 5.5$  Å which corresponds to the bending

parameter larger than one,  $C = 1.06$ . As a result, only a small fraction of the incident electrons (less than 10 per cent) is accepted, and channels over the distance less than  $\lambda_u/2$  having very small amplitude of channeling oscillations,  $a_{ch} \ll d/2$ . Therefore, these particles virtually do not emit ChR but contribute to the CUR part of the spectrum (see the dashed curve in the graph). However, this contribution is not a dominant one. The main part of the peak intensity in the total spectrum comes from the non-channeling particles, see the dash-dotted curve. The explanation is as follows. As discussed above, a trajectory of a non-channeling particle consists of short segments corresponding to VR separated by segments  $\Delta z \approx \lambda_u/2$  where it moves in the over-barrier mode. In the course of two sequential VR the particle experiences 'kicks' in the opposite directions, see the lower trajectory in Fig. 8(a)). Therefore, the whole trajectory becomes modulated periodically with the period  $2\Delta z \approx \lambda_u$ . This modulation gives rise to the emission in the same frequency as CUR.

We believe, that the effects due to the interplay of different radiation mechanisms in PBC can be probed experimentally. In this connection we mention recent successful experiments on detection the excess of radiation in the emission spectra due to VR of 855 MeV electrons in oriented crystal bent with constant curvature [39].

## 5 Conclusions

In this work the channeling and radiation phenomena of 270 and 855 MeV electrons and positrons in  $L_{cr} = 20$  μm thick straight and periodically bent oriented diamond(110) crystals has been simulated by means of the MBN EXPLORER software package [3, 48].

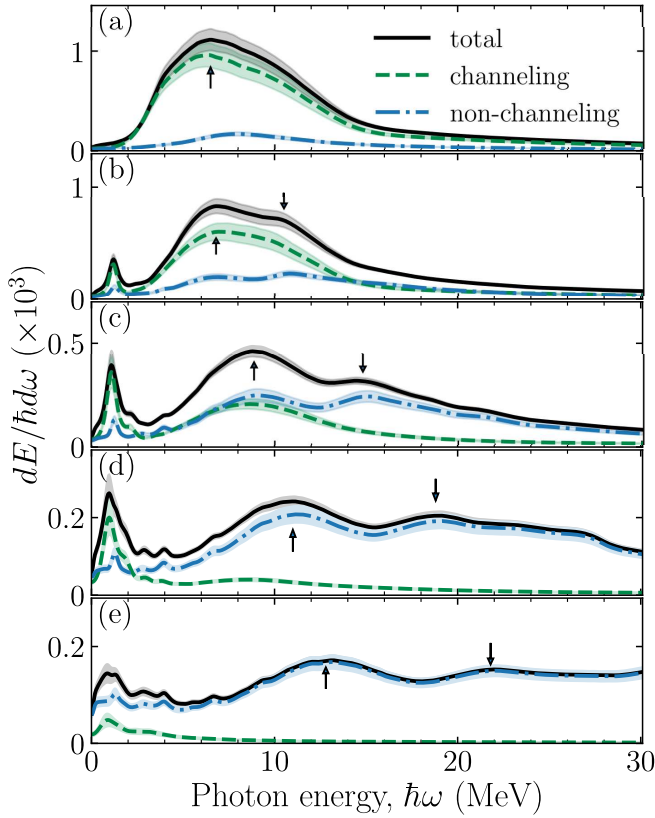


**Fig. 8.** Spectral distributions of radiation emitted by 855 MeV electrons in straight, (a), and periodically bent, (b)-(e), oriented diamond(110) crystal. Graphs (b)-(e) correspond to the bending amplitude  $a = 1.2, 2.5, 4.0, 5.5$  Å, respectively. In each graph the solid black curve indicates the total spectrum, the solid green curve shows the contribution from channeling segments, and dashed blue – from all non-channeling segments (i.e., the over-barrier and the VR ones). The upward arrows indicate the maxima attributed to the ChR (in the straight crystal) and to the interplay of ChR and VR (in the PBC). The downward arrows show the position of the additional maxima appearing in the PBC due to the emission by over-barrier particles. Shading indicates the statistical error due to the finite number of simulated trajectories. The data refer to the opening angle  $\theta_0 = 0.24$  mrad.

Comparison of the emission spectra computed for two different opening angles,  $\theta_0 = 0.24$  and  $4$  mrad, has shown that although higher radiation intensity can be achieved for the larger opening angle, the use of the smaller aperture allows one to distinguish more peculiar features in the spectra.

It has been demonstrated that the CUR spectral density for both positrons and electrons are non-monotonous functions of bending amplitude  $a$  and projectile energy  $\varepsilon$ , so that one can find the optimal parameters which maximize the yield of CUR. This result is important for the experimental studies of the radiation from CUs as well as for designing and practical realization of periodically bent crystalline structures as the key element of the novel CU-based light sources.

Another important result of the analysis is that it is possible to vary the intensity of ChR by choosing the bending amplitude and projectile energy. For positrons, ChR virtually disappears for the projectiles with energy 855 MeV at much lower values of  $a$  than for 270 MeV. This provides an opportunity to decrease the intensity of ChR while keeping high yield of CUR. This effect can be utilized to reduce the radiative energy losses which are mainly due to ChR in oriented crystals. Low radiative energy losses maintain the stability of CUR [60]. The effects predicted in this paper can be measured in the experiments with sub-GeV positron beams. Such beam is available at the DAΦNE facility but some upgrades which will improve the beam quality are desired [61].

For electrons, it has been shown that the intensity of CUR is much smoother function of bending amplitude. It has been demonstrated that in the regime of large bending amplitudes the non-channeling particles provide significant contribution resulting in additional structures in the emission spectra. These rather pronounced effects can be experimentally measured during using the high-quality electron beam available at the MAMI facility [31, 38, 50].

## 6 Acknowledgements

The work was supported in part by the Alexander von Humboldt Foundation Linkage Grant and by the HORIZON 2020 RISE-PEARL project. We acknowledge the Supercomputing Center of Peter the Great Saint-Petersburg Polytechnic University (SPbPU) for providing the opportunities to carry out large-scale simulations. We are grateful to Hartmut Backe and Werner Lauth (University of Mainz) for useful discussions. We are grateful to Referees for the constructive suggestions which lead to significant improvement of the manuscript.

## Author contribution statement

A.V.P. participated in setting up the parameters of CUs to study and conducted a major part of simulations and analysis of the raw data and was the main writer of the paper. A.V.K. participated in setting up the parameters of CUs to study and analysis and discussion of the raw data and final results as well as in writing of the paper. V.K.I. participated in the analysis and discussion of the results. A.V.S. led the studies and interpretation of the results.

## References

1. P. Emma, R. Akre, J. Arthur, R. Bionta, C. Bostedt, J. Bozek, A. Brachmann, P. Bucksbaum, R. Coffee, F.J. Decker et al., *Nature Photonics* **4**, 641 (2010)
2. B.W.J. McNeil, N.R. Thompson, *Nature Photonics* **4**, 814 (2010)

3. I.A. Solov'yov, A.V. Korol, A.V. Solov'yov, *Multiscale modeling of complex molecular structure and dynamics with MBN explorer* (Springer, 2017)
4. K.W.D. Ledingham, P. McKenna, R.P. Singhal, *Science* **300**, 1107 (2003)
5. K.W.D. Ledingham, R.P. Singhal, P. McKenna, I. Spencer, *Europhysics News* **33**, 120 (2002)
6. R. Hajima, T. Hayakawa, N. Kikuzawa, E. Minehara, *Journal of Nuclear Science and Technology* **45**, 441 (2008)
7. J. Lindhard, *Kongel. Dan. Vidensk. Selsk., Mat.-Fys. Medd.* **34** (1965)
8. M.A. Kumakhov, *Phys. Rev. A* **57**, 17 (1976)
9. J.U. Andersen, E. Bonderup, R.H. Pantell, *Annual Review of Nuclear and Particle Science* **33**, 453 (1983)
10. J. Bak, J.A. Ellison, B. Marsh, F.E. Meyer, O. Pedersen, J.B.B. Petersen, E. Uggerhøj, K. Østergaard, S.P. Møller, A.H. Sørensen et al., *Nuclear Physics B* **254**, 491 (1985)
11. U.I. Uggerhøj, *Reviews of modern physics* **77**, 1131 (2005)
12. P.N. Chirkov, Y.A. Chesnokov, V.A. Maisheev, D. Bolognini, S. Hasan, M. Prest, E. Vallazza, *International Journal of Modern Physics A* **31**, 1650051 (2016)
13. E.N. Tsyanov, *Fermilab TM-684* pp. 1 – 8 (1976)
14. J.D. Jackson, *Classical electrodynamics* (John Wiley & Sons, 2012)
15. A.M. Taratin, *Physics of Particles and Nuclei* **29**, 437 (1998)
16. A.V. Solov'yov, A. Schäfer, W. Greiner, *Phys. Rev. E* **53**, 1129 (1996)
17. H. Shen, Q. Zhao, F.S. Zhang, G.B. Sushko, A.V. Korol, A.V. Solov'yov, *Nucl. Instrum. Meth. B* **424**, 26 (2018)
18. A.V. Korol, A.V. Solov'yov, W. Greiner, *J. Phys. G* **24**, L45 (1998)
19. A.V. Korol, A.V. Solov'yov, W. Greiner, *International Journal of Modern Physics E* **8**, 49 (1999)
20. A.V. Korol, A.V. Solov'yov, W. Greiner, *Channeling and Radiation in Periodically Bent Crystals*, 2nd edn. (Springer Verlag, Berlin Heidelberg, 2014)
21. M. Yabashi, H. Tanaka, *Nature Photonics* **11**, 12 (2017)
22. A. Kostyuk, *Phys. Rev. Lett.* **110**, 115503 (2013)
23. A.V. Korol, V.G. Bezchastnov, A.V. Solov'yov, *Eur. Phys. J. D* **71**, 174 (2017)
24. A.V. Korol, V.G. Bezchastnov, G.B. Sushko, A.V. Solov'yov, *Nucl. Instrum. Meth. B* **387**, 41 (2016)
25. G.B. Sushko, A.V. Korol, A.V. Solov'yov, *Nucl. Instrum. Meth. B* **355**, 39 (2015)
26. R.G. Polozkov, V.K. Ivanov, G.B. Sushko, A.V. Korol, A.V. Solov'yov, *Eur. Phys. J. D* **68**, 268 (2014)
27. G.B. Sushko, V.G. Bezchastnov, A.V. Korol, W. Greiner, A.V. Solov'yov, R.G. Polozkov, V.K. Ivanov, *J. Phys.: Conf. Ser.* **438**, 012019 (2013)
28. G.B. Sushko, A.V. Korol, W. Greiner, A.V. Solov'yov, *J. Phys.: Conf. Ser.* **438**, 012018 (2013)
29. A.V. Pavlov, A.V. Korol, V.K. Ivanov, A.V. Solov'yov, *J. Phys. B* **52**, 11LT01 (2019)
30. K.B. Agapev, V.K. Ivanov, A.V. Korol, A.V. Solov'yov, *St. Petersburg State Polytechnical University Journal. Physics and Mathematics* **11** (2), 129 (2018)
31. H. Backe, W. Lauth, T.N. Tran Thi, *Journal of Instrumentation* **13**, C04022 (2018)
32. T.N. Wistisen, U.I. Uggerhøj, J.L. Hansen, W. Lauth, P. Klag, *Eur. Phys. J. D* **71**, 124 (2017)
33. T.N. Wistisen, U.I. Uggerhøj, U. Wienands, T.W. Markiewicz, R.J. Noble, B.C. Benson, T. Smith, E. Bagli, L. Bandiera, G. Germogli et al., *Phys. Rev. Acc. Beams* **19**, 071001 (2016)
34. T.N. Wistisen, K.K. Andersen, S. Yilmaz, R. Mikkelsen, J.L. Hansen, U.I. Uggerhøj, W. Lauth, H. Backe, *Phys. Rev. Lett.* **112**, 254801 (2014)
35. U.I. Uggerhøj, T.N. Wistisen, *Nucl. Instrum. Meth. B* **355**, 35 (2015)
36. U. Wienands, T.W. Markiewicz, J. Nelson, R.J. Noble, J.L. Turner, U.I. Uggerhøj, T.N. Wistisen, E. Bagli, L. Bandiera, G. Germogli et al., *Phys. Rev. Lett.* **114**, 074801 (2015)
37. L. Bandiera, E. Bagli, G. Germogli, V. Guidi, A. Mazzolari, H. Backe, W. Lauth, A. Berra, D. Lietti, M. Prest et al., *Phys. Rev. Lett.* **115**, 025504 (2015)
38. H. Backe, W. Lauth, *Nucl. Instrum. Meth. B* **355**, 24 (2015)
39. A. Mazzolari, E. Bagli, L. Bandiera, V. Guidi, H. Backe, W. Lauth, V. Tikhomirov, A. Berra, D. Lietti, M. Prest et al., *Phys. Rev. Lett.* **112**, 135503 (2014)
40. E. Bagli, L. Bandiera, V. Bellucci, A. Berra, R. Camatari, D. De Salvador, G. Germogli, V. Guidi, L. Lanzoni, D. Lietti et al., *Eur. Phys. J. C* **74**, 3114 (2014)
41. H. Backe, W. Lauth, *Channeling Experiments with Electrons at the Mainz Microtron MAMI*, in *4th Int. Conf. "Dynamics of Systems on the Nanoscale" (Bad Ems, Germany, Oct. 3-7 2016) Book of Abstracts* (2016), p. 58
42. U. Mikkelsen, E. Uggerhøj, *Nucl. Instrum. Methods Phys. Res. B* **160**, 435 (2000)
43. W. Krause, A.V. Korol, A.V. Solov'yov, W. Greiner, *Nucl. Instrum. Methods Phys. Res. A* **483**, 455 (2002)
44. U. Wienands, *Channeling of electrons and positrons at SLAC*, in *"Channeling 2016 - Charged&Neutral Particles Channeling Phenomena" (Sirmione del Garda, Italy, Sept. 25-30 2016)* (2016)
45. U. Wienands, S. Gessner, M. Hogan, T. Markiewicz, T. Smith, J. Sheppard, U. Uggerhøj, J. Hansen, T. Wistisen, E. Bagli et al., *Nucl. Instrum. Meth. B* **402**, 11 (2017)
46. D. Boshoff, M. Copeland, F. Haffeejee, Q. Kilbourn, C. Mercer, A. Osatov, C. Williamson, P. Sihoyiya, M. Motsoai, C.A. Henning et al., *The Search for Diamond Crystal Undulator Radiation*, in *4th Int. Conf. "Dynamics of Systems on the Nanoscale" (Bad Ems, Germany, Oct. 3-7 2016) Book of Abstracts* (2016), p. 38
47. T.N. Tran Thi, J. Morse, D. Caliste, B. Fernandez, D. Eon, Härtwig, *Journal of applied crystallography* **50**, 561 (2017)
48. I.A. Solov'yov, A.V. Yakubovich, P.V. Nikolaev, I. Volkovets, A.V. Solov'yov, *J. Comput. Chem.* **33**, 2412 (2012)
49. G.B. Sushko, V.G. Bezchastnov, I.A. Solov'yov, A.V. Korol, W. Greiner, A.V. Solov'yov, *J. of Comp. Phys.* **252**, 404 (2013)
50. H. Backe, *Journal of Instrumentation* **13**, C02046 (2018)
51. G. Moliere, *Zeitschrift für Naturforschung A* **2**, 133 (1947)
52. V.N. Baier, V.M. Katkov, V.M. Strakhovenko, *Electromagnetic processes at high energies in oriented single crystals* (World Scientific, Singapore, 1998)
53. T.N. Wistisen, A. Di Piazza, *Phys. Rev. D* **99**, 116010 (2019)
54. J. Bak, J.A. Ellison, B. Marsh, F.E. Meyer, *Nucl. Phys. B* **254**, 491 (1985)

55. A.M. Taratin, S.A. Vorobiev, Phys. Lett. A **119**, 425 (1987)
56. A.M. Taratin, S.A. Vorobiev, Nucl. Instrum. Methods Phys. Res. B **26**, 512 (1987)
57. N. Shul'ga, V. Boyko, A. Esaulov, Phys. Lett. A **372**, 2065 (2008)
58. D.F. Alferov, Y.A. Bashmakov, P.A. Cherenkov, Physics-Uspekhi **32**, 200 (1989)
59. V.M. Biryukov, Y.A. Chesnokov, V.I. Kotov, *Crystal channeling and its application at high-energy accelerators* (Springer Science & Business Media, 2013)
60. A.V. Korol, A.V. Solov'yov, W. Greiner, Int. J. Mod. Phys. E **9**, 77 (2000)
61. H. Backe, D. Krambrich, W. Lauth, B. Buonomo, S.B. Dabagov, G. Mazzitelli, L. Quintieri, H. Lundsgaard J, U.I. Uggerhøj, B. Azadegan et al., Nuovo Cimento C **34**, 175 (2011)